PROCEEDINGS OF SCIENCE

Simulating Meson Scattering in (1+1)D $\mathbb{Z}_2$ Lattice Gauge Theory: Efficient Operator Construction and Quantum Circuit Implementation

Yahui Chai,[a,*] **Yibin Guo**[a] **and Stefan Kühn**[a]

[a] *Deutsches Elektronen-Synchrotron DESY, Platanenallee 6, 15738 Zeuthen, Germany*

E-mail: yahui.chai@desy.de, yibin.guo@desy.de, stefan.kuehn@desy.de

We present a framework for efficiently preparing meson wave packets for a lattice gauge theory on quantum devices. The method is demonstrated using a (1+1)D $\mathbb{Z}_2$ lattice gauge theory coupled to Kogut-Susskind staggered fermions as a testbed. Our approach systematically constructs mesonic excitations on top of the ground state with well-defined momentum. Using a *quantum subspace expansion* approach with a symmetry-preserving basis, we obtain explicit operators for creating such excitations, which in turn allow us to construct localized wave packets. By simulating the scattering process of two meson wave packets with Tensor Network States, we identify both elastic and inelastic scattering processes during the dynamics. In addition, we also provide a resource-efficient decomposition for the operators creating mesonic wave packets into elementary quantum gates, thus enabling quantum simulation of meson scattering in the (1+1)D $\mathbb{Z}_2$ lattice gauge theory.

The European Physical Society Conference on High Energy Physics (EPS-HEP2025)
7-11 July 2025
Marseille, France

*Speaker

https://pos.sissa.it/

PoS(EPS-HEP2025)627

1. Introduction

Scattering processes are fundamental for understanding the structure of matter. Lattice gauge theory (LGT) provides a powerful framework for addressing such systems [1], yet simulating their real-time dynamics from first principles remains challenging for classical methods [2, 3]. Using the Lagrangian formulation in Euclidean spacetime lattice, Monte Carlo techniques have been successfully used for estimating static observables, but suffer from the sign problem when extended to real-time [4]. Tensor-network methods, based on the Hamiltonian formulation, offer an alternative approach that enables the direct simulation of quantum dynamics. While they address the sign problem and have produced promising results in (1+1)-dimensional ((1+1)D) LGT [5], their applicability is eventually constrained by the rapid growth of entanglement [6]. Quantum simulation offers a promising alternative [7, 8], as they are free from both the sign problem and entanglement-growth constraints.

Meson scattering in LGT represents a typical process for probing the dynamical properties of gauge theories [1]. As a first step toward higher-dimensional systems, demonstrations in (1+1)D LGT provide a practical testbed for newly developed algorithms while offering rich physics in their own right. Simulating meson scattering on quantum devices faces two key challenges. The first is the construction of high-fidelity particle-creation operators with specific quantum numbers. The second is the realization of non-unitary wave-packet–creation operations within unitary quantum circuits, where the non-unitarity arises from the Gaussian-weighted linear combination of creation operators across different momenta.

Here, we address both challenges through two key technical developments, demonstrated in detail using the (1+1)D $\mathbb{Z}_2$ gauge theory [9]. First, we employ the *quantum subspace expansion* (QSE) [10] to extract optimal coefficients for fermion-antifermion operators with different Wilson-line lengths, in order to construct mesons with well-defined quantum numbers. Second, we construct meson wave packets as Gaussian-weighted linear combinations of these optimized meson creation operators and develop an efficient unitary circuit decomposition based on Givens rotations [11, 12]. The resulting circuit for a system of size L has a depth of $O(L)$ and contains $O(L^2)$ two-qubit gates, making it feasible for NISQ-era hardware and generalizable to other lattice gauge theories. Using matrix product states (MPS), the collision of two mesonic wave packets is explored revealing the rich physical phenomena related to elastic and inelastic scattering processes.

2. Model and Method

The Hamiltonian of the (1+1)D $\mathbb{Z}_2$ lattice gauge theory [9] with staggered fermions [13] on a periodic lattice with L matter sites is given by

$$H = \frac{1}{2a}\sum_{n=1}^{L}\left(\xi_n^\dagger Z_{g,n}\xi_{n+1} + \text{h.c.}\right) + m\sum_{n=1}^{L}(-1)^n \xi_n^\dagger \xi_n + \varepsilon\sum_{n=1}^{L} X_{g,n}, \tag{1}$$

where ξ_n ($\xi_n^\dagger$) is the fermionic annihilation (creation) operator for site n, and the Pauli operators $Z_{g,n}$ and $X_{g,n}$ act on the $\mathbb{Z}_2$ gauge link between sites n and $n+1$. The parameters m and ε denote the fermion mass and the coupling strength, respectively. The lattice spacing a is set to 1 for the

PoS(EPS-HEP2025)627

rest of the paper. Physical states $|\psi\rangle$ must satisfy the Gauss law constraint, $\forall n\ G_n |\psi\rangle = |\psi\rangle$, where

$$G_n = X_{g,n-1}\, e^{i\pi Q_n}\, X_{g,n}, \quad Q_n = \xi_n^\dagger \xi_n - \frac{1-(-1)^n}{2}. \tag{2}$$

The QSE is used to construct high-fidelity meson-creation operators with well-defined and well-controlled quantum numbers such as momentum. The ansatz for a meson-creation operator is

$$b_{k,c}^\dagger = \sum_{n,\ell=1}^{L} a_{n\ell}^{(k,c)}\, \xi_n^\dagger W_{n,\ell} \xi_\ell, \tag{3}$$

where $W_{n,\ell}$ is the Wilson line connecting sites n and ℓ, chosen along the shorter of the two paths on the periodic lattice to ensure gauge invariance. The parameters k and $c = \pm 1$ label the lattice momentum and the charge conjugation eigenvalue, respectively.

To determine the coefficients $a_{n\ell}^{(k,c)}$, we solve a generalized eigenvalue problem in the subspace spanned by $M_I |\Omega\rangle$, where $|\Omega\rangle$ denotes the gauge-invariant ground state of H and $M_I \equiv \xi_n^\dagger W_{n,\ell} \xi_\ell$ with the multi-index $I \in (n, \ell)$. Representing the coefficients $a_{n\ell}^{(k,c)}$ as a vector $\vec{a}^{(k,c)}$, the resulting generalized equation takes the form

$$(\mathcal{H} + \mathcal{C} + \mathcal{Z})\, \vec{a}^{(k,c)} = \lambda \mathcal{S}\, \vec{a}^{(k,c)}, \tag{4}$$

where $\mathcal{H}$, $\mathcal{C}$, $\mathcal{Z}$, and $\mathcal{S}$ are matrices whose elements are defined as

$$\mathcal{H}_{IJ} = \langle\Omega| M_I^\dagger H M_J |\Omega\rangle, \qquad \mathcal{C}_{IJ} = \langle\Omega| M_I^\dagger C M_J |\Omega\rangle, \tag{5}$$
$$\mathcal{Z}_{IJ} = \langle\Omega| M_J M_I^\dagger |\Omega\rangle, \qquad \mathcal{S}_{IJ} = \langle\Omega| M_I^\dagger M_J |\Omega\rangle. \tag{6}$$

$\mathcal{C}_{IJ}$ is included to ensure that the resulting states are simultaneous eigenstates of the Hamiltonian and the charge-conjugation operator, which commute with each other. The term $\mathcal{Z}$ in the QSE equation penalizes components arising from annihilation operators $b_{k,c}$ that act nontrivially on the vacuum, thereby enforcing the condition $b_{k,c}|\Omega\rangle \approx 0$. After normalizing the eigenvector such that $\vec{a}^\dagger \mathcal{S} \vec{a} = 1$, we extract the physical energy E, the charge-conjugation expectation value with phase ce^{-ik}, and the annihilation norm $\mathcal{N}_{\mathcal{Z}}$ from the expectation values

$$E = \vec{a}^{(k,c)\dagger} \mathcal{H} \vec{a}^{k,c}, \quad ce^{-ik} = \vec{a}^{(k,c)\dagger} \mathcal{C} \vec{a}^{(k,c)}, \quad \mathcal{N}_{\mathcal{Z}} = \vec{a}^{(k,c)\dagger} \mathcal{Z} \vec{a}^{(a,c)}.$$

We refer to the quantities obtained through this procedure as the QSE results and to the overall procedure as the QSE method.

Once the meson creation operators are constructed, we use them to build localized wave packets and simulate meson-meson scattering. A single meson wave packet with mean momentum $\bar{k}$ and mean position $\bar{x}$ is created by applying the creation operator $B_{\bar{k},\bar{x}}^\dagger$ to the vacuum $|\Omega\rangle$. Here we focus on the vector mesons with $c = -1$. The explicit form of this operator is

$$B_{\bar{k},\bar{x}}^\dagger = \sum_{k\in\Lambda^*} \phi_{\bar{k},\bar{x}}(k)\, b_{k,-1}^\dagger, \quad \phi_{\bar{k},\bar{x}}(k) = \frac{1}{\sqrt{\mathcal{N}_\phi}}\, e^{-ik\bar{x}}\, e^{-(k-\bar{k})^2/(4\sigma_k^2)}, \tag{7}$$

where Λ^* is the truncated momentum basis used to construct the wave packet, σ_k its width in momentum space, and $\mathcal{N}_\phi$ normalizes the wave packet. The operator $B_{\bar{k},\bar{x}}^\dagger$ creates a vector meson wave packet.

PoS(EPS-HEP2025)627

The system is initialized in the state $|\psi(0)\rangle = B^{\dagger}_{\bar{k},x_1} B^{\dagger}_{-\bar{k},x_2} |\Omega\rangle$, corresponding to two mesons with opposite momenta and allowing us to study two-particle scattering. The positions x_1 and x_2 are chosen far apart to ensure that the two meson wave packets are initially well separated. We simulate the dynamics of wave packets by employing a second-order Trotter decomposition of the evolution operator. All simulations are performed using the open-source ITensor library [14]. During the simulations, as well as in the later quantum computing approach, the fermionic operators are mapped to spin degrees of freedom by the Jordan-Wigner transformation, $\xi^{\dagger}_n = \prod_{l<n}(-iZ_l)(X_n+iY_n)/2$ [15]. To characterize the scattering process, we monitor the subtracted site-resolved staggered fermion density defined as $\Delta\langle\chi_n\rangle \equiv \langle\psi(t)|\chi_n|\psi(t)\rangle - \langle\Omega|\chi_n|\Omega\rangle$, where $\chi_n \equiv (-1)^n Q_n$.

3. Results

3.1 State Preparation

To benchmark the QSE method, we first compute the vacuum $|\Omega\rangle$ using MPS. We then obtain the eigenstates in the QSE subspace and the relevant quantities, using again the MPS formalism. For comparison, we also directly compute excited states with the MPS method by adding penalty terms that shift the energy of previously obtained lower-energy eigenstates upward, ensuring orthogonality to earlier states [16]. An additional diagonalization step is performed to resolve degenerate states with opposite momentum, since translation invariance forces states with nonvanishing momentum to occur in pairs with $\pm k$. For the scaling analysis in Fig. 1, we further diagonalize the subspace spanned by all low-energy MPS reference states, which improves the accuracy of the MPS estimates at large system sizes. For simulating scattering dynamics, we adopt a Trotterized time evolution as discussed previously.[1]

We present the scaling behavior for two different momentum modes, $k = 0$ and $k = 2\times(2\pi/N)$ in Fig. 1. The system size ranges from 20 to 60 sites in steps of 10, with parameters $m = 0.3$ and $\varepsilon = 0.3$. The Wilson-line length in the fermion-antifermion operators in Eq. (3) is restricted to separations shorter than 10 in order to reduce computational cost. This approximation is justified by the fact that confinement localizes mesonic excitations to a small spatial region [17]. Figure 1(a) shows the infidelity of the QSE results with respect to the direct MPS computation. As the figure suggests, the infidelity increases only marginally with system size, and all fidelities remain above 99.9%.

Figures 1(b) and (c) indicate the relative energy fluctuation $\Delta E/|E|$ and the fluctuation of charge conjugation value ΔC, respectively, where $\Delta O = \sqrt{|\langle O^2\rangle - \langle O\rangle^2|}$ for an observable O. Both quantities should vanish for an exact eigenstate. The values of $\Delta E/|E|$ and ΔC obtained from QSE are close to zero. Although the $\Delta E/|E|$ from QSE is larger than MPS results for small system sizes and comparable for large system sizes, the ΔC values from QSE are consistently lower than those from MPS. This indicates that the QSE-obtained states are close to true eigenstates and exhibit better behavior with respect to the desired symmetry.

[1] For computing excited states, we set the cutoff parameter in ITensor to 10^{-10}, for dynamical simulations, we set it to 10^{-9}.

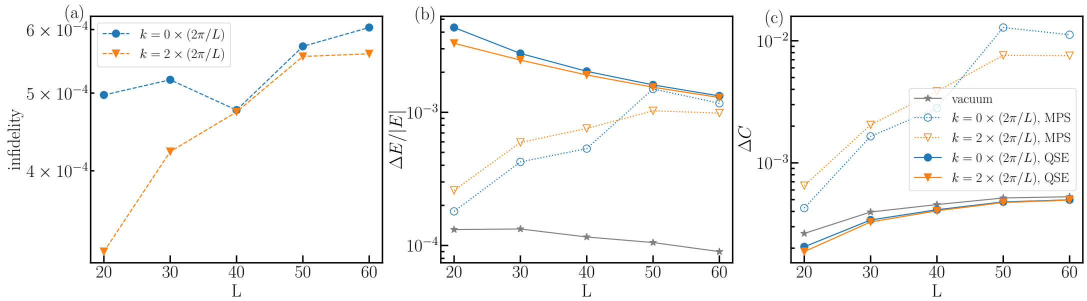

Figure 1: Scaling behavior of the QSE with system size up to 60 sites (120 qubits) for $m = 0.3$ and $\varepsilon = 0.3$, and momentum $k = 0 \times (2\pi/L)$ and $k = 2 \times (2\pi/L)$. (a) Infidelity relative to the reference MPS. (b) Relative energy fluctuation, and (c) charge-conjugation fluctuation for states from QSE and for the reference MPS.

3.2 Elastic Meson Scattering

Let us first consider the strong-coupling regime, $\varepsilon/m \gg 1$. Without loss of generality, we choose parameters of $m = 0.1$ and $\varepsilon = 1.0$ for a system size $L = 30$ as an example. Figure 2(a) shows the energy-momentum dispersion of the 28 lowest-energy mesons obtained from QSE method and from MPS simulations. The plot presents the energy difference ΔE between the excited states and the ground state as a function of momentum. The charge-conjugation expectation value c (without the associated phase) indicates that all these excitations are vector mesons. As shown in the figure, the ΔE values obtained from QSE and MPS simulations are in excellent agreement.

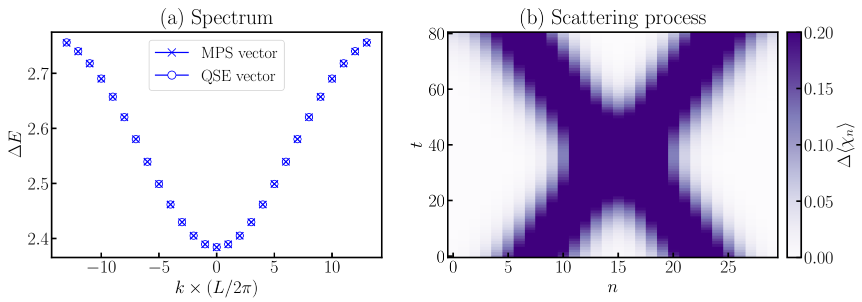

Figure 2: Observations for the system with $L = 30$, $m = 0.1$, and $\varepsilon = 1.0$. (a) Energy-momentum dispersion of the 28 lowest-energy mesons, showing the energy difference ΔE between the excited states and the ground state for different momenta. (b) Time evolution of the staggered fermion density $\Delta\langle\chi_n\rangle$ during the elastic scattering of two vector mesons with momentum $\pm 6 \times (2\pi/L)$, and wave packet width $\sigma_k = 2\pi/L$.

Now we create two vector mesons using the computed set of 28 vector-meson creation operators and evolve them in time to simulate the scattering process. Figure. 2(b) shows the time evolution of the spatial distribution of the staggered fermion density $\Delta\langle\chi_n\rangle$. The two mesons are initially centered at positions $x_1 = 8$ and $x_2 = 23$, with momenta $\pm 6 \times (2\pi/L)$. As time evolves, the two wave packets approach each other and undergo a collision at time $t \approx 34$. After the collision, two outgoing mesons appear with the same internal structure as the incoming ones. Since no new particles are produced, the process is identified as elastic scattering.

3.3 Inelastic Meson Scattering

Then we turn to the intermediate coupling regime. As an example, we choose parameters of $m = 0.2$ and $\varepsilon = 0.2$ for a system size $L = 30$. Figure 3(a) shows the energy-momentum dispersion of the 30 lowest-energy mesons, where both vector ($c = -1$) and scalar ($c = 1$) branches appear. The figure compares the results obtained from the QSE method with those from MPS simulations. The vector meson energy excess above the vacuum ΔE shows excellent agreement between QSE and MPS, while the agreement for the scalar mesons is slightly worse but still remains accurate.

The vector meson wave packets with high momentum $\bar{k} = 8 \times (2\pi/L)$ are prepared with the computed 21 vector meson-creation operators. The high momentum is chosen such that the total incoming energy exceeds the scalar meson mass, enabling the generation of new particles. As shown in Fig. 3(b), the two vector meson wave packets are prepared at positions $x_1 = 8$ and $x_2 = 23$. The collision occurs at $t = 20 \sim 40$ and leads to the formation of two slower-moving scalar mesons, along with residual vector-meson components. This suggests that the scattering process is inelastic.

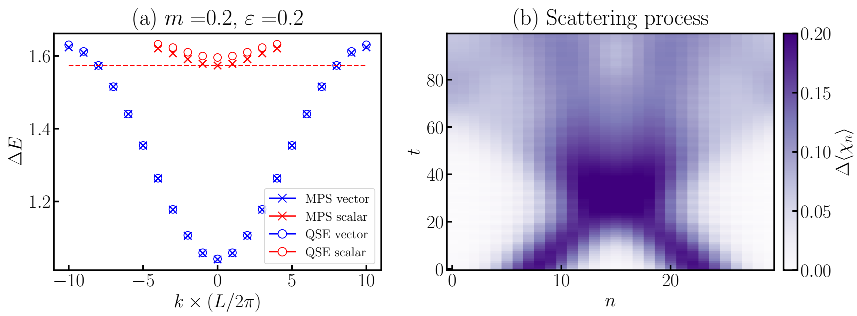

Figure 3: Observations for the system with $L = 30$, $m = 0.2$, and $\varepsilon = 0.2$. (a) Energy-momentum dispersion of the 30 lowest-energy mesons, showing the energy difference ΔE between the excited states and the ground state for different momenta. (b) Time evolution of the staggered fermion density $\Delta\langle\chi_n\rangle$ during the inelastic scattering of two vector mesons with momentum $k = \pm 8 \times (2\pi/L)$, wave packet width $\sigma_k = 2\pi/L$, where scalar-meson production is observed.

4. Circuit Implementation

To prepare meson wave packets on a digital quantum computer, we construct an efficient circuit. The meson creation operator in Eq. (7) is non-Hermitian. Thus, we introduce a Hermitian operator $A^\dagger_{\bar{k},\bar{x}} \equiv B^\dagger_{\bar{k},\bar{x}} + B_{\bar{k},\bar{x}}$, which satisfies $A^\dagger_{\bar{k},\bar{x}}|\Omega\rangle = B^\dagger_{\bar{k},\bar{x}}|\Omega\rangle$. This condition is enforced in our QSE construction. Numerically, we find a fidelity above 99.9% between the two resulting states, thus justifying this replacement.

The implementation of $A^\dagger_{\bar{k},\bar{x}}$ proceeds in two steps. Figure 4 shows the circuit for the case $L = 4$. First, by introducing $\tilde{\xi}_n \equiv W_{1,n}\xi_n$, the operator can be written as $A^\dagger_{\bar{k},\bar{x}} = \sum_{nlr} \tilde{\xi}^\dagger_n (u_{nr} D_{rr} u^\dagger_{rl})\tilde{\xi}_l$ and diagonalized as

$$A^\dagger_{\bar{k},\bar{x}} = V(u) O_D V(u)^\dagger, \tag{8}$$

where

$$V(u) = \exp\left(\sum_{nl} \tilde{\xi}_n^\dagger \,[\log u]_{nl}\, \tilde{\xi}_l\right), \quad O_D = \sum_r \lambda_r \tilde{\xi}_r^\dagger \tilde{\xi}_r. \tag{9}$$

In a second step, O_D is implemented via a Hadamard test using the unitary operators O_a and O_b, which reproduce O_D through their anti-commutator up to an overall normalization.

All operators $V(u)$, O_a and O_b are decomposed using Givens rotations. For the details, we refer to Ref. [18]. Here, we ignore single-qubit gates for the phase of each matrix element and summarize the structure at the level of rotation layers. As Fig. 4 shows, the first (last) block corresponds to $V(u)^\dagger$ ($V(u)$). Sharp- and round-corner squares distinguish unitary gates that are related by a conjugate transpose. Each rotation requires 4 CNOT gates due to the gauge-link contribution. Consequently, a single $V(u)$ consists of $L(L-1)/2$ rotations with depth $2L-3$, requiring $2L(L-1)$ CNOT gates and a depth of $4(2L-3)$. In contrast, O_a and O_b require $2(L-1)$ rotations, where each rotation in O_a uses 2 CNOTs and each in O_b uses 6 CNOTs in both count and depth. This leads to $4(L-1)$ and $12(L-1)$ in both CNOT count and depth for O_a and O_b, respectively. Altogether, the circuit uses $4L^2 + 16L - 20$ CNOT gates and has a depth of $36L - 44$, excluding the two CNOTs used in the Hadamard test. When $L \gg 1/\sigma_k$, the scaling with L can be replaced by $1/\sigma_k$. Further resource reductions are possible by parallelization or by utilizing higher connectivity in quantum devices.

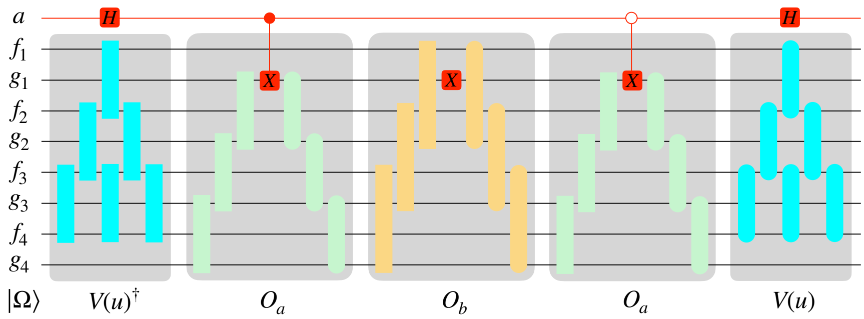

Figure 4: Meson wave-packet preparation circuit for $L = 4$, implementing $A^\dagger_{\bar{k},\bar{x}}$ starting from the vacuum $|\Omega\rangle$. The blocks show (i) diagonalization via $V(u)$ and (ii) implementation of O_D using a Hadamard test on O_a and O_b (up to normalization). Givens rotations decompose $V(u)$, O_a, and O_b; single-qubit gates are omitted. Sharp- and round-corner squares indicate gates related by a conjugate transpose. The circuit uses $4L^2 + 16L - 20$ CNOTs with depth $36L - 44$, excluding the two Hadamard-test CNOTs.

5. Summary and Outlook

In this talk, we propose a non-variational framework for preparing meson wave packets and simulating their dynamics on quantum devices. Using a generalized QSE procedure, we construct a symmetry-preserving basis and meson creation operators and demonstrate this method for the (1+1)D $\mathbb{Z}_2$ LGT with staggered fermions studying both elastic and inelastic scattering processes. The observed scaling behavior of the QSE results with system size suggests scalability to larger systems. We also develop efficient quantum circuits for preparing meson wave-packet states using elementary gates. The framework introduced here should also be applicable to more complicated LGTs, such as the Schwinger model and higher-dimensional systems. In addition, we plan on evaluating the performance on real quantum hardware in the future.

References

[1] J.C. Halimeh, N. Mueller, J. Knolle, Z. Papić and Z. Davoudi, *Quantum simulation of out-of-equilibrium dynamics in gauge theories*, *arXiv preprint arXiv:2509.03586* (2025) .

[2] A. Di Meglio, K. Jansen, I. Tavernelli, C. Alexandrou, S. Arunachalam, C.W. Bauer et al., *Quantum computing for high-energy physics: State of the art and challenges*, *PRX Quantum* **5** (2024) 037001.

[3] C.W. Bauer, Z. Davoudi, A.B. Balantekin, T. Bhattacharya, M. Carena, W.A. De Jong et al., *Quantum simulation for high-energy physics*, *PRX Quantum* **4** (2023) 027001.

[4] G. Pan and Z.Y. Meng, *The sign problem in quantum Monte Carlo simulations*, Elsevier (2024), 10.1016/b978-0-323-90800-9.00095-0.

[5] M.C. Bañuls, K. Cichy, J.I. Cirac, K. Jansen and S. Kühn, *Tensor networks and their use for lattice gauge theories*, *PoS(LATTICE 2018)022* (2019) .

[6] T. Xiang, *Density Matrix and Tensor Network Renormalization*, Cambridge University Press (2023), 10.1017/9781009398671.

[7] I.M. Georgescu, S. Ashhab and F. Nori, *Quantum simulation*, *Rev. Mod. Phys.* **86** (2014) 153.

[8] A.J. Daley, I. Bloch, C. Kokail, S. Flannigan, N. Pearson, M. Troyer et al., *Practical quantum advantage in quantum simulation*, *Nature* **607** (2022) 667.

[9] D. Horn, M. Weinstein and S. Yankielowicz, *Hamiltonian approach to $z(n)$ lattice gauge theories*, *Phys. Rev. D* **19** (1979) 3715.

[10] N. Yoshioka, H. Hakoshima, Y. Matsuzaki, Y. Tokunaga, Y. Suzuki and S. Endo, *Generalized quantum subspace expansion*, *Phys. Rev. Lett.* **129** (2022) 020502.

[11] W. Givens, *Computation of plain unitary rotations transforming a general matrix to triangular form*, *Journal of the Society for Industrial and Applied Mathematics* **6** (1958) 26.

[12] J.J. Vartiainen, M. Möttönen and M.M. Salomaa, *Efficient decomposition of quantum gates*, *Phys. Rev. Lett.* **92** (2004) 177902.

[13] J. Kogut and L. Susskind, *Hamiltonian formulation of Wilson's lattice gauge theories*, *Phys. Rev. D* **11** (1975) 395.

[14] M. Fishman, S.R. White and E.M. Stoudenmire, *The ITensor Software Library for Tensor Network Calculations*, *SciPost Phys. Codebases* (2022) 4.

[15] C.J. Hamer, Z. Weihong and J. Oitmaa, *Series expansions for the massive schwinger model in hamiltonian lattice theory*, *Phys. Rev. D* **56** (1997) 55.

[16] M.C. Bañuls, K. Cichy, K. Jansen and J.I. Cirac, *The mass spectrum of the schwinger model with matrix product states*, *J. High Energy Phys.* **2013** (2013) 158.

PoS(EPS-HEP2025)627

[17] Z. Davoudi, C.-C. Hsieh and S.V. Kadam, *Quantum computation of hadron scattering in a lattice gauge theory*, 2505.20408.

[18] Y. Chai, Y. Guo and S. Kühn, *Towards Quantum Simulation of Meson Scattering in a Z2 Lattice Gauge Theory*, *arXiv preprint arXiv:2505.21240* (2025) .